Proper formation of whisker barrelettes requires periphery-derived Smad4-dependent TGF-β signaling

Susana da Silva[a,b], Hiroshi Hasegawa[a,1], Alexandra Scott[a], Xiang Zhou[a], Amanda K. Wagner[a], Bao-Xia Han[a], and Fan Wang[a,2]

[a]Department of Cell Biology, Duke University Medical Center, Durham, NC 27710; and [b]Doctoral Program in Experimental Biology and Biomedicine, Center for Neuroscience and Cell Biology, University of Coimbra, 3004-517 Coimbra, Portugal

Edited by Eve Marder, Brandeis University, Waltham, MA, and approved January 19, 2011 (received for review September 24, 2010)

Mammalian somatosensory topographic maps contain specialized neuronal structures that precisely recapitulate the spatial pattern of peripheral sensory organs. In the mouse, whiskers are orderly mapped onto several brainstem nuclei as a set of modular structures termed barrelettes. Using a dual-color iontophoretic labeling strategy, we found that the precise topography of barrelettes is not a result of ordered positions of sensory neurons within the ganglion. We next explored another possibility that formation of the whisker map is influenced by periphery-derived mechanisms. During the period of peripheral sensory innervation, several TGF-β ligands are exclusively expressed in whisker follicles in a dynamic spatiotemporal pattern. Disrupting TGF-β signaling, specifically in sensory neurons by conditional deletion of *Smad4* at the late embryonic stage, results in the formation of abnormal barrelettes in the principalis and interpolaris brainstem nuclei and a complete absence of barrelettes in the caudalis nucleus. We further show that this phenotype is not derived from defective peripheral innervation or central axon outgrowth but is attributable to the misprojection and deficient segregation of trigeminal axonal collaterals into proper barrelettes. Furthermore, *Smad4*-deficient neurons develop simpler terminal arbors and form fewer synapses. Together, our findings substantiate the involvement of whisker-derived TGF-β/Smad4 signaling in the formation of the whisker somatotopic maps.

One prominent characteristic of the rodent whisker-somatosensory system is its precisely organized topographic sensory maps (1–3). Each whisker is innervated by peripheral axons of a subset of trigeminal sensory neurons whose cell bodies reside in the trigeminal ganglia (TG) and central axons project to the brainstem (4). Sensory afferents carrying information from individual whiskers segregate and converge to form modular structures termed barrelettes, whose spatial organization exactly mirrors that of the whiskers in the periphery (5). The barrelette map in the brainstem emerges during development and serves as a template for the subsequent generation of homologous upstream structures in the thalamus and cortex, termed barreloids and barrels, respectively (5, 6). Interestingly, induction of an extra whisker by exogenous expression of Shh during early development leads to the formation of an extra barrelette with a topographic position corresponding to that of the ectopic whisker (7). Together with other studies (8–10), these data suggest that the formation of the whisker map is under the strong instructive influence of the periphery. The whisker-derived signals regulating barrelette formation remain mostly unknown, however.

Previous work showed that BMP4 signaling induces differential expression of genes in trigeminal sensory neurons innervating different areas of the face along the dorsoventral axis (11, 12). At later developmental stages, multiple TGF-β superfamily ligands are expressed in whisker follicles during the period of sensory axon innervation (12–14). Retrograde TGF-β signaling has been shown to regulate neural development in *Drosophila*, including the growth and plasticity of the neuromuscular junction (15–17) and the specification of FMRFamide-expressing neurons (18, 19). To investigate whether whisker-derived TGF-β signaling plays an essential role in orchestrating barrelette map formation in the mouse, we deleted the gene encoding Smad4, a required downstream factor for TGF-β signal transduction, specifically in sensory neurons. The detailed analyses and general implications of our study are presented and discussed here.

Results

Cell Bodies of Sensory Neurons Innervating Neighboring Whiskers Are Intermingled in the TG. We devised a method to analyze the topography of whisker-innervating sensory neurons with high spatial resolution. Iontophoretic injection of fluorophore-tagged dextrans into whisker follicles of newborn mice [postnatal day (P) 0] allows the visualization of sensory neuron cell bodies and their central axonal projections (Fig. 1). To test whether neurons innervating neighboring whiskers along the same whisker row (D2 and D3) are presegregated within the TG, we injected each whisker with Dextran-Alexa568 (red) and Dextran-Alexa488 (green). This resulted in differential labeling of the corresponding barrelettes in all brainstem nuclei at P3 (Fig. 1*D*). The segregation of "red" and "green" axons into neighboring barrelettes confirms the specificity of each injection. Interestingly, we observe that the barrelette map formed in the spinal nucleus caudalis (SpC) has an opposite orientation compared with the maps formed in the spinal nucleus interpolaris (SpI) and trigeminal principalis (PrV) along the lateral-medial (L-M) axis (Fig. 1*D*).

Strikingly, despite the clear segregation of central projections in the brainstem, the cell bodies of D2 and D3 whisker-innervating neurons display a scattered and intermingled distribution in the TG (Fig. 1*C* and Fig. S1*B*). This unexpected finding indicates that there is a topographic discontinuity in the somatotopic representation of neighboring whiskers in the TG. To address if this discontinuity is specific for adjacent whiskers along the anterior-posterior (A-P) axis, we performed dual labeling of whiskers located at opposite edges of the same row (C1/C5) and neighboring whiskers across rows (C3/D3) (Fig. S1 *C* and *D*). Analysis of different whisker pairs revealed that the degree of cell body segregation for C3/D3 innervating neurons is considerably higher than that for D2/D3 neurons [segregation index (SI) $_{C3/D3}$ = 0.47, $P < 0.001$; $SI_{D2/D3}$ = 0.06, $P = 0.84$; calculations of SI are presented in *SI Methods* and Fig. S1]. This coarse segregation of cell bodies along the dorsal-ventral (D-V) axis is consistent with previous studies (11, 20). Nevertheless, in all whisker pairs analyzed, a considerable fraction of cell bodies from the two neuronal populations were scattered and intermingled within the TG. Moreover, we detected no sorting or differential fasciculation of central axon tracts before their termination into barrelettes (Fig. S1*A*). These results suggest that the precise somatotopy achieved during whisker map formation

Author contributions: S.d.S., H.H., and F.W. designed research; S.d.S., H.H., A.S., A.K.W., and B.-X.H. performed research; X.Z. contributed new reagents/analytic tools; S.d.S., H.H., X.Z., and F.W. analyzed data; and S.d.S. and F.W. wrote the paper.

The authors declare no conflict of interest.

This article is a PNAS Direct Submission.

[1]Present address: Graduate School of Comprehensive Human Sciences, University of Tsukuba, Tsukuba 305-0006, Japan.

[2]To whom correspondence should be addressed. E-mail: f.wang@cellbio.duke.edu.

This article contains supporting information online at www.pnas.org/lookup/suppl/doi:10.1073/pnas.1014411108/-/DCSupplemental.

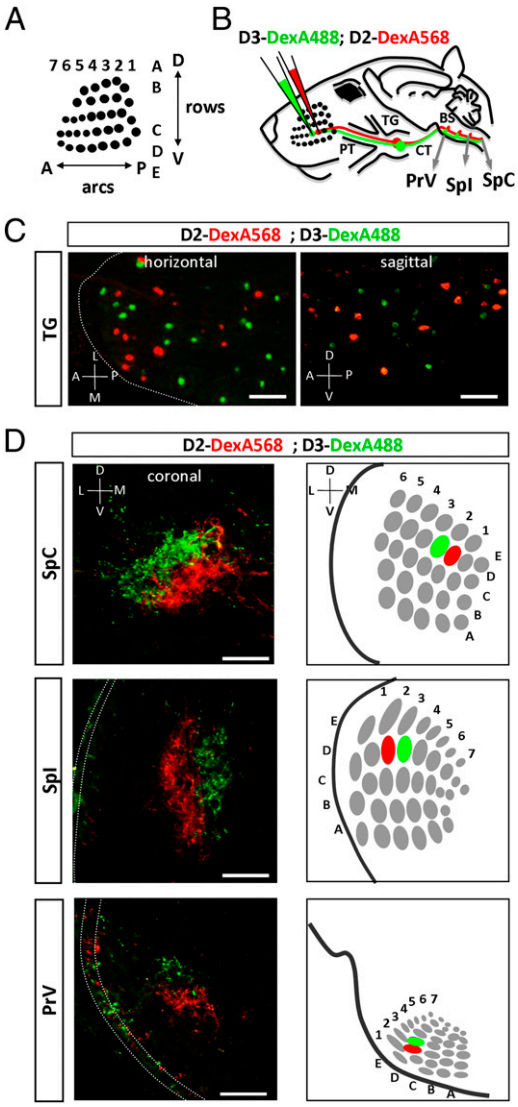

Fig. 1. Trigeminal sensory neurons innervating neighboring whiskers are intermingled and scattered in the TG. (*A*) Schematic diagram of the topographic arrangement of large whiskers in the mouse face. Whiskers are organized in five rows (A–E) along the D-V axis and in up to seven arcs (1–7) along the A-P axis. (*B*) D2 and D3 whiskers were injected with Dextran-fluorophore tagged with either Alexa568 or Alexa488 at P0. Injections resulted in labeling of cell bodies and axon projections of trigeminal sensory neurons. (*C*) Horizontal and sagittal sections of TG 3 d after injection of mice with dual-labeled D2 and D3 whiskers reveal that cell bodies of neurons innervating adjacent whiskers are intermingled in the ganglion. (*D*) Coronal sections of SpC, SpI, and PrV nuclei at P3 reveal clear segregation of central axon projections of D2- and D3-innervating neurons into two distinct barrelettes. Note that the whisker map in the SpC is represented with an opposite orientation compared with the maps in the SpI and PrV. BS, brainstem; CT, central tract; DexA488, Dextran-Alexa488; DexA568, Dextran-Alexa568. (Scale bars: *C*, 100 μm; *D*, 50 μm.)

is not attributable to presegregation of sensory neurons within the ganglion.

TGF-β Ligands Are Exclusively Expressed in the Whisker Pad During Trigeminal Development. Previous work from our laboratory has shown that BMP4, a member of the TGF-β superfamily, retrogradely induces transcriptional changes in trigeminal sensory neurons during early development (11). This led us to examine the expression pattern of other TGF-β superfamily members during follicle development. At embryonic day (E) 16.5, a time point when sensory neurons have innervated whisker follicles and are sending collaterals into central regions, *Activin A*, *Bmp2*, *Bmp4*, *Bmp7* (Fig. 2*A*), *TGF-β1*, and *TGF-β2* (Fig. S2*A*) are all extensively expressed in whisker follicles. Importantly, none of the corresponding ligands is detected in the TG or brainstem nuclei, indicating that they are exclusively expressed in the periphery (Fig. 2*A*). At E14.5, *Activin A* mRNA forms a gradient along the A-P axis with high expression levels in the posterior whiskers and relatively low levels in the anterior whiskers (Fig. 2*B*). Interestingly, the *Activin A* expression pattern is temporally dynamic and shifts between E12.5 and E14.5 (Fig. S2*B*). This period of spatially dynamic *Activin A* expression slightly proceeds and overlaps with the formation of trigeminal central collaterals and the central whisker maps in the brainstem (21) (Fig. S2*C*). Thus, Activin A and other TGF-β ligands are at the right time and in the right place to influence trigeminal central axonal projections through retrograde signaling.

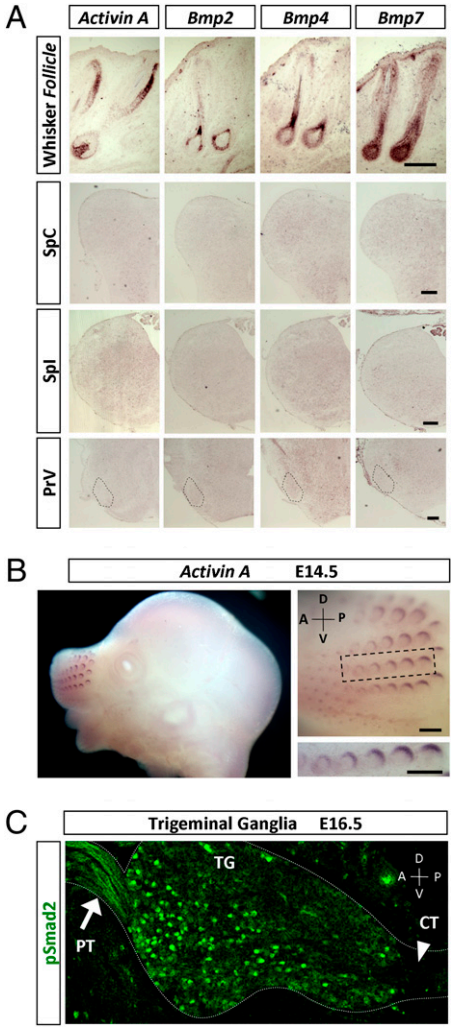

Fig. 2. TGF-β ligand expression in the whisker pad and activation of TGF-β signaling in trigeminal sensory neurons. (*A*) In situ hybridization of *Activin A*, *Bmp2*, *Bmp4*, and *Bmp7* in the whisker pad and in SpC, SpI, and PrV brainstem nuclei at E16.5. Dashed lines delineate the PrV nucleus. All transcripts are exclusively expressed in the whisker follicles. (*B*) Whole-mount in situ hybridization of *Activin A* at E14.5 reveals its expression in the whisker pad. Note the gradient established by the differential expression among whisker follicles along the A-P axis. (*Lower Right*) Magnified view of whisker row D. (*C*) pSmad2 immunolabeling of TG at E16.5 shows robust signal of pSmad2 in the cell bodies and axons of the PT (arrow) but not in the axons of the CT (arrowhead). CT, central tract. (Scale bars: *A*, 200 μm; *B*, 100 μm.)

To examine whether TGF-β signaling is activated in developing trigeminal sensory neurons, we analyzed the levels of phospho-Smad2 (pSmad2) by immunocytochemistry. The phosphorylation of Smad2 is triggered by binding of TGF-β ligands to TGF-β receptors (22). At E16.5, subsets of trigeminal neurons in the maxillary region of the TG exhibit a robust nuclear pSmad2 signal (Fig. 2*C* and Fig. S3*A*), which colocalizes with NeuN labeling (Fig. S3*B*). The distribution of pSmad2-positive neurons in the TG is scattered and sparse (Fig. 2*C*), resembling the pattern of neurons innervating single whiskers (Fig. 1*C*). Importantly, pSmad2 is detected in the peripheral tract (PT) of the maxillary branch of the TG but not in the central axon tract (Fig. 2*C*). Moreover, pSmad2 signal is absent by P1 (Fig. S3*A*). This indicates that retrograde activation of this pathway occurs primarily during the period of whisker map development in late embryos. Furthermore, we observe variable levels of pSmad2 among different neurons, suggesting differential levels of TGF-β pathway activation across the trigeminal neuron population (Fig. 2*C* and Fig. S3).

Generation of Mice with Impaired TGF-β Signaling in Sensory Neurons by Conditional Deletion of Smad4. To test whether TGF-β signaling is involved in the formation of barrelette maps, we specifically deleted *Smad4* gene in sensory neurons during whisker map development. Smad4 is a common downstream component of the signaling cascade activated by the TGF-β superfamily (22). This strategy overcomes the extensive promiscuity between TGF-β ligands and receptors and the multiple downstream receptor-associated Smads activated by TGF-β signals (22, 23). Furthermore, to delete Smad4 specifically in sensory neurons and preserve the normal development of whisker follicles, we crossed $Smad4^{flox/flox}$ mice with the sensory-specific Cre line, $Advillin^{Cre/+}$ (Fig. 3*A*) (21) (Fig. S4). $Advillin^{Cre/+}$-mediated gene deletion was characterized using a Cre reporter line $Rosa26Sor^{tm1(CAG-ALPP)Fawa}$ ($Rosa^{PLAP}$) (24, 25), in which a high level of human placenta alkaline phosphatase (PLAP) is induced by Cre recombinase. $Advillin^{Cre/+}$-mediated PLAP expression in trigeminal sensory neurons begins at E12.5 and is present in most neurons around E15.5 (Fig. S4*B*), a time when most trigeminal central collaterals start to project into the brainstem nuclei (4, 11, 21). In situ hybridization in Smad4-cKO ($Advillin^{cre/+}$; $Smad4^{flox/flox}$) TG confirmed the loss of *Smad4* mRNA in sensory neurons from E14.5 onward (Fig. 3*B* and Fig. S4*C*).

Abnormal Barrelette Formation in Smad4-cKO Mice. To test whether *Smad4* deletion in sensory neurons affects barrelette formation, we performed cytochrome oxidase (CO) staining on brainstem sections of control ($Advillin^{cre/+}$; $Smad4^{flox/+}$ or $Advillin^{cre/+}$ mice) and Smad4-cKO mice at P1. In control mice, CO staining revealed segregated barrelettes in all three brainstem nuclei: SpI (Fig. 3*C*), PrV (Fig. S5*A*), and SpC (Fig. S5*B*). In contrast, only weak and diffuse CO staining signals were observed in Smad4-cKO brainstem nuclei, with no distinct barrelettes (Fig. 3*C* and Fig. S5 *A* and *B*).

In control mice, barrelettes develop sharper boundaries and expand in size during the first postnatal week (Fig. 3*C*). During the same period, small and irregular-shaped barrelette-like structures appear in the Smad4-cKO SpI and PrV nuclei (Fig. 3*C* and Fig. S5*A*). Furthermore, in the SpC nucleus, no discernible structures are ever detected in Smad4-cKO mice (Fig. S5*B*). This complete lack of barrelette formation in the mutant SpC was further verified by immunolabeling against TenascinC, an extracellular matrix protein (Fig. 3*D*).

To assess the development of barrelette synaptic structures, we labeled postsynaptic sites and all presynaptic termini of trigeminal axons by NR2B and vGlut1 immunostaining, respectively (26, 27). Both staining results were consistent with and recapitulated the pattern observed using CO staining, further confirming the abnormality of barrelettes in Smad4-cKO mice (Fig. 3*E* and Fig. S5 *C–E*). Moreover, the overall fluorescence intensity of vGlut1 measured in SpI at P7 was decreased by 40% (Fig. S5*F*), suggesting that there are fewer synapses generated in

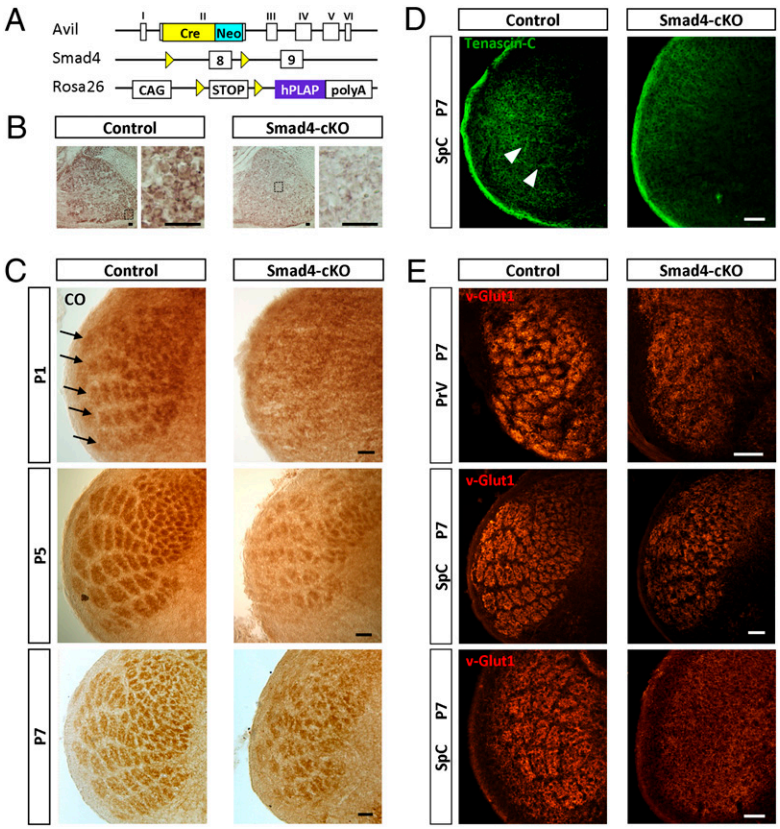

Fig. 3. Smad4-cKO sensory neurons form defective barrelettes. (*A*) Schematic of the alleles used to generate [$Advillin^{cre/+}$; $Smad4^{flox/flox}$] mice: $Advillin^{Cre}$, $Smad4^{flox}$, and $ROSA26Sor^{tm1(CAG-ALPP)Fawa}$ ($Rosa^{PLAP}$). (*B*) In situ hybridization of *Smad4* in Smad4-cKO mice at E15.5 confirms the deletion of *Smad4* in trigeminal sensory neurons. Magnified view (*Right*) of the regions highlighted (*Left*). (*C*) CO staining of control and Smad4-cKO SpI nucleus at P1, P5, and P7. Note that at P1, barrelettes are distinguishable in control SpI (arrows) but imperceptible in Smad4-cKO SpI. At later stages, barrelette-like structures emerge in Smad4-cKO SpI, but defined barrelettes are never observed. (*D*) TenascinC immunostaining (green) of a P7 SpC nucleus. In control mice, barrelette boundaries are revealed by TenascinC (arrowheads), whereas in Smad4-cKO mice, this pattern is lost. (*E*) vGlut1 immunolabeling (red) of PrV, SpI, and SpC of P7 control and Smad4-cKO mice. vGlut1 staining reveals the emergence of barrelette-like structures in SpI and PrV nuclei and no barrelettes in the SpC nucleus of Smad4-cKO mice. (Scale bars: 100 μm; *B*, enlarged views, 25 μm.)

Smad4-cKO mice. Taken together, these findings indicate that intact TGF-β signaling in trigeminal sensory neurons is essential for the proper formation of the barrelette map.

Normal Peripheral Sensory Innervation and Central Axon Outgrowth of Smad4-cKO Trigeminal Sensory Neurons. The aberrant barrelette formation in Smad4-cKO mice could be attributable to neuronal viability or axon outgrowth defects caused by *Smad4* deletion. To address the viability and differentiation state of Smad4-cKO trigeminal sensory neurons, we examined the pattern and number of neurons expressing transcripts for neurotrophic receptors *TrkA*, *TrkB*, *TrkC*, and *cRet* and differentiation markers *TrpV1*, *TrpM8*, *TrpC3*, *TrpA1*, *Cacna2d3*, and *MrgB4* (Fig. S6 *A–C*) by in situ hybridization. No differences were found between control and Smad4-cKO neurons, except for a mild reduction in the number of neurons expressing *MrgB4* (Fig. S6*C*).

To examine whether peripheral sensory innervation is affected by *Smad4* deletion, we performed immunofluorescence against the specific neuronal marker PGP9.5. *Smad4*-deficient neurons show normal whisker innervation in embryonic and postnatal stages (Fig. 4*A*), with all types of whisker sensory endings (Merkel ending, transverse and longitudinal lanceolate endings, Ruffini/spinal endings, and reticular endings) formed at appropriate positions along the shaft of the hair follicles at apparent normal densities (Fig. 4*A* and Fig. S7*A*).

Furthermore, we assessed axonal outgrowth in vivo by examining the projections of trigeminal axonal collaterals using the $Rosa^{PLAP}$ reporter line (24, 25). No apparent differences were detected in the growth of sensory axonal collaterals into brainstem nuclei between control and mutant mice in embryonic and postnatal stages (Fig. 4*B* and Fig. S7*B*). To exclude possible intrinsic problems in axon elongation further, we analyzed axon length and the number of primary and secondary branches in postnatal in vitro cultures of TG neurons. No difference in axon outgrowth was found between *Smad4*-deleted and control neurons (Fig. S6 *D* and *E*).

Abnormal Topographic Projection and Segregation of Smad4-cKO Sensory Afferents. The aberrant phenotype observed in Smad4-cKO brainstem nuclei may be caused by the misprojection and/or deficient segregation of trigeminal central axons into appropriate barrelettes. To test this hypothesis, we traced central projections from neurons innervating neighboring whiskers using the dual-color labeling method described previously (Fig. 1*B*) and analyzed the extent of overlap between their respective terminal projections in the brainstem. Control and Smad4-cKO D2/D3 whiskers were injected at P0 with Dextran-Alexa568 (red) and Dextran-Alexa488 (green), respectively, and the central axon projections in SpC and SpI nuclei, as well as the extent of overlap between the two labeled populations, were analyzed 3 d later. In the SpC of control mice, the axon termini of neurons innervating D2 and D3 whiskers coalesce and converge to form two clearly distinguishable barrelettes (Fig. 4*C*, *Upper Left*). By contrast, in the SpC of Smad4-cKO mice, central axons from both labeled populations exhibit a more diffuse distribution with no distinct barrelettes (Fig. 4*C*, *Upper Right*). This is consistent with the CO and vGlut1 staining results described previously, wherein no barrelettes were ever detected in this subnucleus (Fig. 3*E* and Fig. S5*B*). Quantitative analysis of terminal projections from each population of labeled neurons revealed that Smad4-cKO axons project to a wider area compared with control neurons (Fig. 4*C* and Fig. S8 *C* and *D*; average projection area in SpC: control, $28{,}476 \pm 10{,}422\ \mu m^2$, $n = 4$; Smad4-cKO, $54{,}970 \pm 9{,}865\ \mu m^2$, $n = 6$; $P < 0.01$). Furthermore, in Smad4-cKO mice, the overlapping projection area of the two labeled axon populations is much larger than that in control mice (Fig. 4*D*; control, $19\% \pm 2.1\%$ overlap, $n = 4$; Smad4-cKO, $40\% \pm 3.4\%$ overlap, $n = 6$; $P < 0.001$).

In the SpI nucleus, where small abnormal barrelette-like structures appear around P3/P4 (Fig. 3*C*), the absolute axonal projection areas from whisker D2 or D3 innervating neurons are similar between mutant and control mice at P3 (Fig. S8 *C* and *E*).

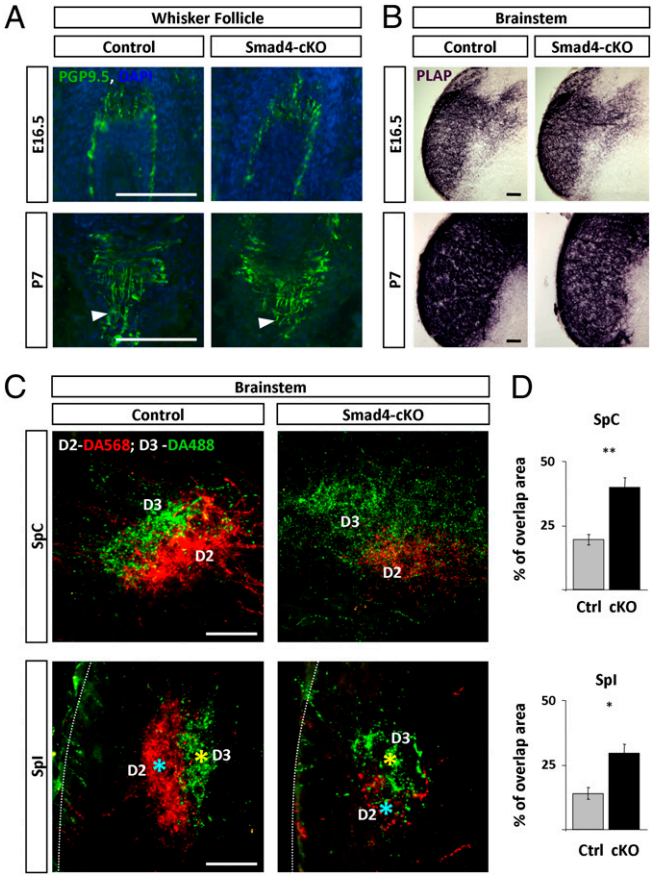

Fig. 4. *Smad4*-cKO sensory neurons have normal peripheral innervation and central axon outgrowth but defective segregation of central projections. (*A*) PGP9.5 immunostaining of whisker follicles at E16.5 and P7 of control and Smad4-cKO mice. Sections were counterstained with DAPI. No difference in whisker sensory innervation is detected between control and Smad4-cKO mice at both time points. Arrowheads indicate longitudinal lanceolate endings at P7. (*B*) PLAP staining of sensory central projections to the SpI at E16.5 and P7 in control and Smad4-cKO mice. No major changes are detected. (*C*) Maximum projection images of confocal stacks depicting dextran-labeled central projections of control and Smad4-cKO sensory neurons innervating D2 and D3 whiskers in SpC (*Upper*) and SpI (*Lower*) nuclei at P3. Asterisks indicate centroids of D2 (blue) and D3 (yellow) corresponding barrelettes. Note that the relative orientation of the two centroids is affected by Smad4 ablation. (*D*) Average ± SEM of the percentage of overlap between labeled barrelettes in SpC and SpI (Ctrl: $n = 3$ mice, cKO: $n = 6$ mice). $^*P < 0.01$; $^{**}P < 0.001$. cKO, Smad4-cKO; Ctrl, control. (Scale bar: 100 μm.)

The percentage of overlap between the projection areas of the two axonal populations is significantly higher in Smad4-cKO mice, however (Fig. 4*D*; control, 14.1% overlap, $n = 4$; Smad4-cKO, 29.5% overlap, $n = 6$; $P < 0.01$). Moreover, the relative positions of the two presumptive barrelettes varied greatly among different Smad4-cKO mice (Fig. 4*C* and Fig. S8*C*). In some cases, the topographic order of the green and red barrelettes was actually reversed (asterisks in Fig. 4*C* and Fig. S8*C*). These results indicate that Smad4-deficient sensory neurons misproject their central axons in the brainstem nuclei.

Smad4-Deleted TG Neurons Have Atrophied Terminal Arborization and Fewer Synaptic Contacts. The disperse pattern of innervation observed in the barrelettes of Smad4-cKO mice could be attributable to either an exaggerated arborization of axon terminals or an actual misprojection of individual axons during development. To visualize the detailed morphology of terminal arbors from individual mechanosensory neurons, we devised

a strategy based on the tamoxifen-inducible CreER-t2 recombinase (28, 29) and the reporter line ROSA^{PLAP}. For this, we generated a unique mouse line with CreER-t2 inserted into the *Advillin* locus (*Advillin*$^{CreERt2/+}$). Single-neuron PLAP labeling was accomplished by two low-dose tamoxifen injections in [*Advillin*$^{CreERt2/+}$; *Smad4*$^{flox/flox}$; *Rosa*$^{PLAP/+}$] mice at E12.5 and E13.5. In cases in which only a single sensory neuron was labeled per whisker, as detected by A-P staining of the whisker pad (examples are shown in Fig. 5*B*), we sectioned the brainstem and reconstructed the axonal trajectory and terminal arbors of those neurons (Fig. 5 *C* and *D*).

Analysis of Neurolucida 3D reconstruction and 2D projections of axon termini in SpI at P1 (Fig. 5 *C*–*F*) indicates that *Smad4*-deleted neurons have fewer and simpler terminal branches compared with control neurons (40% decrease in branch density, 30% decrease in arbor total length, and 45% reduction in varicosity density in Smad4-cKO vs. control neurons) (Fig. 5*G*). The simpler and shorter axon arbors of Smad4-deleted neurons strongly suggest that the diffuse pattern of barrelette innervation in Smad4-cKO mice is attributable to a misprojection and not to overarborization of axon terminals.

Ultrastructural analysis of Smad4-cKO PrV synapses at P7 by EM revealed no difference in synaptic vesicle density, postsynaptic density length, or synaptic cleft width compared with control synapses. This suggests that Smad4 deficiency does not disrupt synapse formation. Moreover, the distribution of asymmetrical Gray type I synapses (Fig. 5*H*, white arrowheads) and symmetrical Gray type II synapses (Fig. 5*H*, red arrows) detected in PrV was unchanged between phenotypes. The overall number of synapses generated by Smad4-cKO neurons was significantly reduced compared with control neurons, however (Fig. 5*I*; 1.85 ± 0.06 synapses per 10 μm^2 in Smad4-cKO, n = 180 boutons, vs. 2.97 ± 0.16 synapses per 10 μm^2 in control neurons, n = 200 boutons; $P < 0.001$). In addition, the average bouton area was 30% smaller in mutant neurons (Fig. 5*I*) and the number of boutons containing multiple synaptic sites was reduced (Fig. 5*H*). These data indicate that *Smad4* deficiency results in a smaller number of synapses being formed. This is consistent with the lower vGlut1 levels detected in the brainstem (Fig. 3*D* and Fig. S5*F*), and the phenotype is likely a secondary consequence of axon misprojection.

Discussion

Previous studies suggest that development of the barrelette map is influenced by periphery-derived signals (7, 11). In this study, we show that TGF-β ligands are spatiotemporal dynamically expressed in whiskers, and Smad4-dependent TGF-β signaling is an important regulator of whisker-somatosensory map development.

Morphogens induce different gene expression programs depending on their concentration (30). In this respect, we found that genes encoding several cell surface receptor molecules, EphA4,

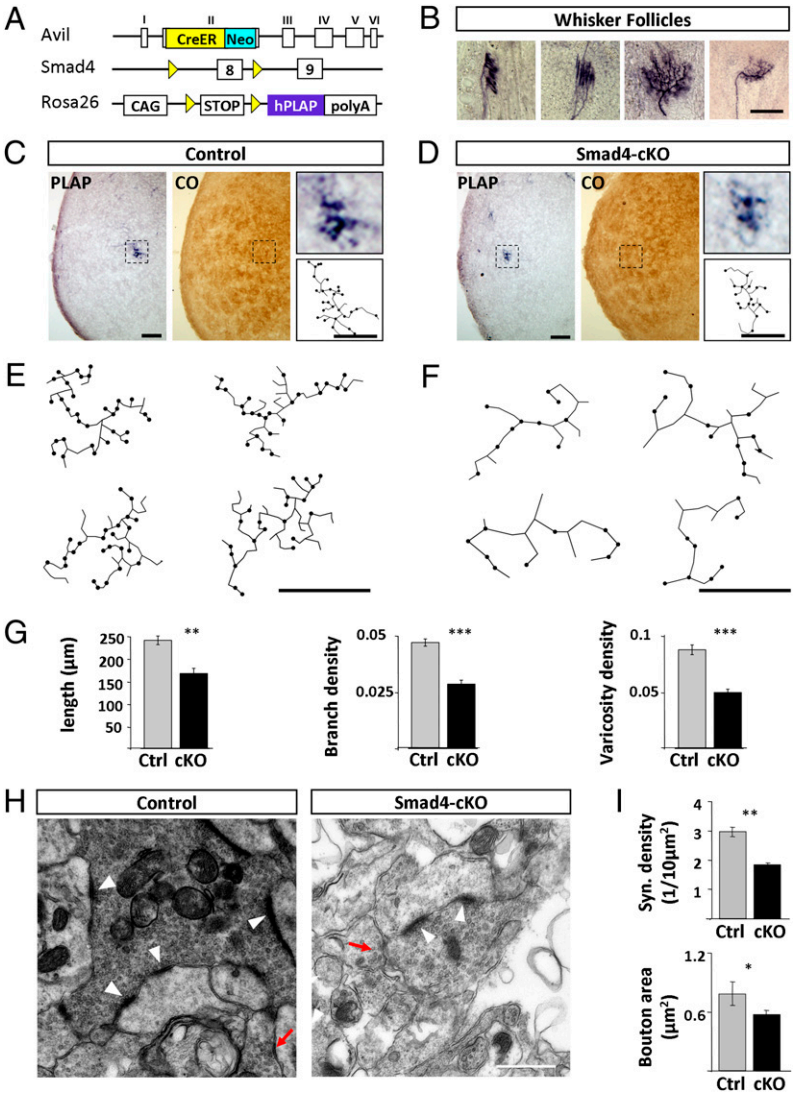

Fig. 5. Atrophied terminal arborization and reduced number of synapses in Smad4-cKO sensory neurons. (*A*) Schematic of the alleles used here. CreERt2 was inserted into the *Advillin* locus to generate *Advillin*^{CreERt2}. The *Advillin*^{CreERt2} line then was crossed with *Smad4*^{flox} and the reporter line *Rosa*^{PLAP}. (*B*) PLAP staining of a single trigeminal mechanosensory neuron innervating one whisker follicle at P1. PLAP and CO staining of consecutive sections of control (*C*) and Smad4-cKO (*D*) SpI nuclei at P1. Magnified view (*Upper Right*) of the central terminal projection highlighted (*Left*). 2D projection (*Lower Right*) of the complete 3D Neurolucida reconstruction of the same terminal arbor. Representative 2D projections of terminal arbors in SpI nucleus of control (*E*) and Smad4-cKO (*F*) mice are shown. The dots (•) represent varicosities, defined as an enlargement of the axon. Note the decreased complexity and fewer varicosities present in Smad4-cKO neurons. (*G*) Quantitative analysis of total length and branch and varicosity densities of Ctrl and cKO terminal arbors (Ctrl: n = 47, four mice; cKO: n = 20, four mice). (*H*) EM images of control and Smad4-cKO terminal boutons of PrV nuclei at P7. White arrowheads indicate asymmetrical synaptic contacts, and red arrows indicate symmetrical contacts. Note the presence of fewer synapses in Smad4-cKO boutons. (*I*) Average ± SEM synaptic density (number of synapses/10 μm^2) and bouton area (μm^2) of cKO (n = 180 boutons) and Ctrl (n = 200 boutons) mice. *$P < 0.05$; **$P < 0.01$; ***$P < 0.001$ by the Student's t test. cKO, Smad4-cKO; Ctrl, control. (Scale bars: *A*–*D*, 100 μm; *C*–*F*, 50 μm in enlarged views; *H*, 500 nm.)

Neurotrimin (Hnt), and Igsf21, exhibit a scattered expression pattern in the maxillary region of the TG (Fig. S9). Importantly, all three genes are down-regulated in Smad4-cKO trigeminal sensory neurons (Fig. S9). These and other yet unidentified cell surface receptors could be the transcriptional targets of TGF-β signaling that mediate the segregation and convergence of sensory afferents in the brainstem.

It is likely that the formation of highly precise somatosensory maps depends on multiple factors and pathways in addition to TGF-β signaling. Different mammalian species exhibit a highly diverse repertoire of peripheral sensory organs with complex structures, which impinge their spatial pattern onto topographic maps formed in the brain (31). Thus, periphery-derived retrograde signaling mechanisms may provide the plasticity and adaptability necessary for the seamless innervation and mapping of complex sensory organs by the somatosensory system.

Methods

Advillin^{Cre} and Advillin^{CreERt2} Mice. Advillin Cre and CreERt2 details of gene targeting strategy are illustrated in Figs. 3 and 5, respectively. The PCR primer used for genotyping are *Avil/003*, 5′-CCCTGTTCACTGTGAGTAGG-3′; *Avil/002*, 5′-AGTATCTGGTAGGTGCTTCCAG; and *Cre/01*, 5′-GCGATCCCTGAACATGTC-CATC. WT allele produces a 500-bp fragment (*Avil/003* and *Avil/002*), and mutant allele results in a 180-bp fragment (*Avil/003* and *Cre/01*). Note that only the *Advillin^{Cre}* male (but not female) mouse is useful for sensory neuron-specific *Cre* expression. For activation of CreERt2 in *Advillin^{CreERt2}*, 2 mg of tamoxifen (T-5648; Sigma) dissolved in corn oil was injected i.p. into pregnant female mice at E12.5 and E13.5. *Smad4$^{flox/flox}$* and *Rosa26R-CAG-STOP-hPLAP* mice (*Rosa^{PLAP}*) have been described previously (24, 25). All experiments were conducted according to protocols approved by the Duke University Institutional Animal Care and Use Committee.

Iontophoretic Injection of Dextran-Alexa Conjugates. Dextran amine (10,000 M_r) conjugated to either Alexa568 or Alexa488 [5% (wt/vol); Molecular Probes/Invitrogen] was iontophoreticaly injected into a whisker in anesthetized neonatal (P0) mice. A negative 20-μA current with a pulse width of 10 ms was delivered at 30 Hz to the microcapillary pipette. Details on the quantitative analyses of dextran-injected samples are provided in *SI Methods* and Fig. S1.

Histological Analyses. Section and whole-mount in situ hybridization and alkaline phosphatase staining were performed as previously described. CO staining was performed as previously explained (32). Immunofluorescence was carried out using standard procedure. Primary antibodies were anti-vGlut1 antibody (1:5,000; Millipore), anti-TenascinC antibody [1:1,000; a gift from Harold Erickson, Duke University, Durham, NC (33)], anti-NR2B (1:250; Upstate), anti-PGP9.5 (1:1,000; Ultraclone), anti-NeuN (1:100, Millipore), anti-NF200 (1:400; Sigma), and antiphosphorylated-Smad2 (1:200; Cell Signaling). A full description of the methods used is provided in *SI Methods*.

ACKNOWLEDGMENTS. We thank Dr. Leonard White for help with the Neurolucida procedure. We thank Rui Peixoto and Dr. Ian Davison for assistance in establishing the iontophoretic injection system and Dr. Ehlers for sharing the iontophoretic injection equipment. We thank Dr. Sara Miller and Phillip Christopher for helping with transmission EM. We also thank the Duke Transgenic Mouse Facility for performing blastocyst injections to generate the *Advillin^{cre}* and *Advillin^{CreER}* knock-in mouse lines. We thank Rui Peixoto, members of the F.W. laboratory, Dr. Scott Soderling, and Dr. Guoping Feng for critically reading and commenting on this manuscript. This work was supported by the McKnight Scholar Award, the Wings for Life Foundation, and National Institutes of Health Grants DE16550 and DE19440A1 from the National Institute of Dental and Craniofacial Research (all to F.W.). S.d.S. was supported by a predoctoral fellowship from the Foundation for Science and Technology, Portugal.

1. Woolsey TA, Van der Loos H (1970) The structural organization of layer IV in the somatosensory region (SI) of mouse cerebral cortex. The description of a cortical field composed of discrete cytoarchitectonic units. *Brain Res* 17:205–242.
2. Killackey HP, Rhoades RW, Bennett-Clarke CA (1995) The formation of a cortical somatotopic map. *Trends Neurosci* 18:402–407.
3. Petersen CC (2007) The functional organization of the barrel cortex. *Neuron* 56: 339–355.
4. Erzurumlu RS, Murakami Y, Rijli FM (2010) Mapping the face in the somatosensory brainstem. *Nat Rev Neurosci* 11:252–263.
5. Killackey HP, Fleming K (1985) The role of the principal sensory nucleus in central trigeminal pattern formation. *Brain Res* 354:141–145.
6. Ding YQ, Yin J, Xu HM, Jacquin MF, Chen ZF (2003) Formation of whisker-related principal sensory nucleus-based lemniscal pathway requires a paired homeodomain transcription factor, Drg11. *J Neurosci* 23:7246–7254.
7. Ohsaki K, Nakamura S (2006) Instructive role of a peripheral pattern for the central patterning of the trigeminal projection at the brainstem and thalamus revealed by an artificially altered whisker pattern. *Neuroscience* 141:1899–1908.
8. Chiaia NL, et al. (1996) Effect of neonatal axoplasmic transport attenuation in the infraorbital nerve on vibrissae-related patterns in the rat's brainstem, thalamus and cortex. *Eur J Neurosci* 8:1601–1612.
9. Van der Loos H, Welker E, Dörfl J, Rumo G (1986) Selective breeding for variations in patterns of mystacial vibrissae of mice. Bilaterally symmetrical strains derived from ICR stock. *J Hered* 77:66–82.
10. Durham D, Woolsey TA (1984) Effects of neonatal whisker lesions on mouse central trigeminal pathways. *J Comp Neurol* 223:424–447.
11. Hodge LK, et al. (2007) Retrograde BMP signaling regulates trigeminal sensory neuron identities and the formation of precise face maps. *Neuron* 55:572–586.
12. Bitgood MJ, McMahon AP (1995) Hedgehog and Bmp genes are coexpressed at many diverse sites of cell-cell interaction in the mouse embryo. *Dev Biol* 172:126–138.
13. Lyons KM, Pelton RW, Hogan BL (1989) Patterns of expression of murine Vgr-1 and BMP-2a RNA suggest that transforming growth factor-beta-like genes coordinately regulate aspects of embryonic development. *Genes Dev* 3:1657–1668.
14. Takahashi H, Ikeda T (1996) Transcripts for two members of the transforming growth factor-beta superfamily BMP-3 and BMP-7 are expressed in developing rat embryos. *Dev Dyn* 207:439–449.
15. McCabe BD, et al. (2003) The BMP homolog Gbb provides a retrograde signal that regulates synaptic growth at the Drosophila neuromuscular junction. *Neuron* 39: 241–254.
16. Ball RW, et al. (2010) Retrograde BMP signaling controls synaptic growth at the NMJ by regulating trio expression in motor neurons. *Neuron* 66:536–549.
17. Goold CP, Davis GW (2007) The BMP ligand Gbb gates the expression of synaptic homeostasis independent of synaptic growth control. *Neuron* 56:109–123.
18. Allan DW, St Pierre SE, Miguel-Aliaga I, Thor S (2003) Specification of neuropeptide cell identity by the integration of retrograde BMP signaling and a combinatorial transcription factor code. *Cell* 113:73–86.
19. Marqués G, et al. (2003) Retrograde Gbb signaling through the Bmp type 2 receptor wishful thinking regulates systemic FMRFa expression in Drosophila. *Development* 130:5457–5470.
20. Erzurumlu RS, Jhaveri S (1992) Trigeminal ganglion cell processes are spatially ordered prior to the differentiation of the vibrissa pad. *J Neurosci* 12:3946–3955.
21. Hasegawa H, Abbott S, Han BX, Qi Y, Wang F (2007) Analyzing somatosensory axon projections with the sensory neuron-specific Advillin gene. *J Neurosci* 27: 14404–14414.
22. Massagué J (1998) TGF-beta signal transduction. *Annu Rev Biochem* 67:753–791.
23. Massagué J (2000) How cells read TGF-beta signals. *Nat Rev Mol Cell Biol* 1:169–178.
24. Kessler JD, et al. (2009) N-myc alters the fate of preneoplastic cells in a mouse model of medulloblastoma. *Genes Dev* 23:157–170.
25. Que J, et al. (2008) Mesothelium contributes to vascular smooth muscle and mesenchyme during lung development. *Proc Natl Acad Sci USA* 105:16626–16630.
26. Magnusson KR, Larson AA, Madl JE, Altschuler RA, Beitz AJ (1986) Co-localization of fixative-modified glutamate and glutaminase in neurons of the spinal trigeminal nucleus of the rat: An immunohistochemical and immunoradiochemical analysis. *J Comp Neurol* 247:477–490.
27. Clements JR, Beitz AJ (1991) An electron microscopic description of glutamate-like immunoreactive axon terminals in the rat principal sensory and spinal trigeminal nuclei. *J Comp Neurol* 309:271–280.
28. Feil R, Wagner J, Metzger D, Chambon P (1997) Regulation of Cre recombinase activity by mutated estrogen receptor ligand-binding domains. *Biochem Biophys Res Commun* 237:752–757.
29. Indra AK, et al. (1999) Temporally-controlled site-specific mutagenesis in the basal layer of the epidermis: Comparison of the recombinase activity of the tamoxifen-inducible Cre-ER(T) and Cre-ER(T2) recombinases. *Nucleic Acids Res* 27:4324–4327.
30. Tabata T, Takei Y (2004) Morphogens, their identification and regulation. *Development* 131:703–712.
31. Catania KC, Henry EC (2006) Touching on somatosensory specializations in mammals. *Curr Opin Neurobiol* 16:467–473.
32. Li Y, Erzurumlu RS, Chen C, Jhaveri S, Tonegawa S (1994) Whisker-related neuronal patterns fail to develop in the trigeminal brainstem nuclei of NMDAR1 knockout mice. *Cell* 76:427–437.
33. Settles DL, Kusakabe M, Steindler DA, Fillmore H, Erickson HP (1997) Tenascin-C knockout mouse has no detectable tenascin-C protein. *J Neurosci Res* 47:109–117.